Supplementary Information (SI) for Physical Chemistry Chemical Physics.
This journal is © the Owner Societies 2025

Supporting Information for Phase diagram and dynamics of edge oxidation of C_3N monolayer in O_2 atmospheres from first-principles calculations

Zhongyue Li, Nan Zhao, Haitao Chen† and Liang Zhao†

[a]College of Physical Science and Technology, Yangzhou University, Jiangsu, 225009, China

†Corresponding authors: htchen@yzu.edu.cn; zhaoliang@yzu.edu.cn

PS. 1. Atomic charges at C_3NNR edges

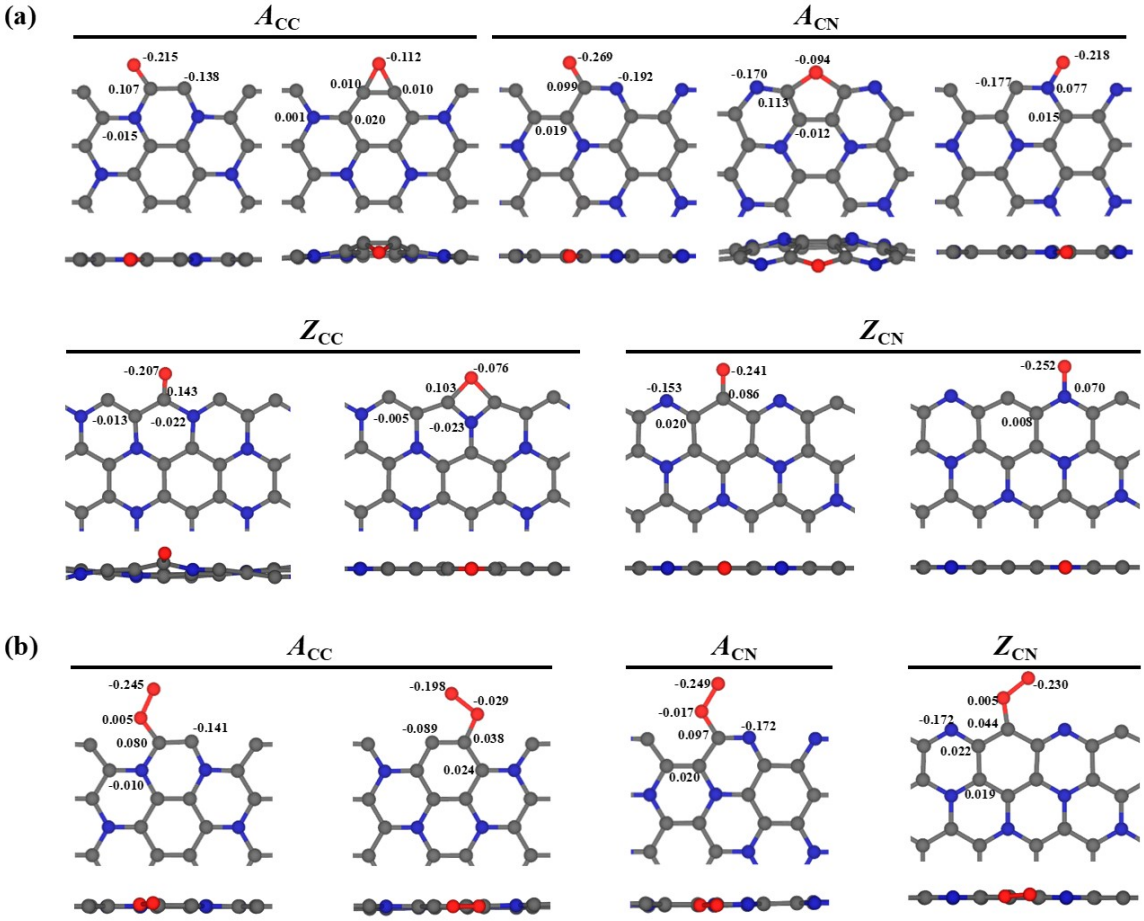

Figure S1. Hirshfeld charges of (a) single atomic O or (b) an O_2 chemisorbed at C_3NNR edges, in the unit of *e*.

PS. 2. All the optimized oxidation configurations for four types of C_3NNR edges

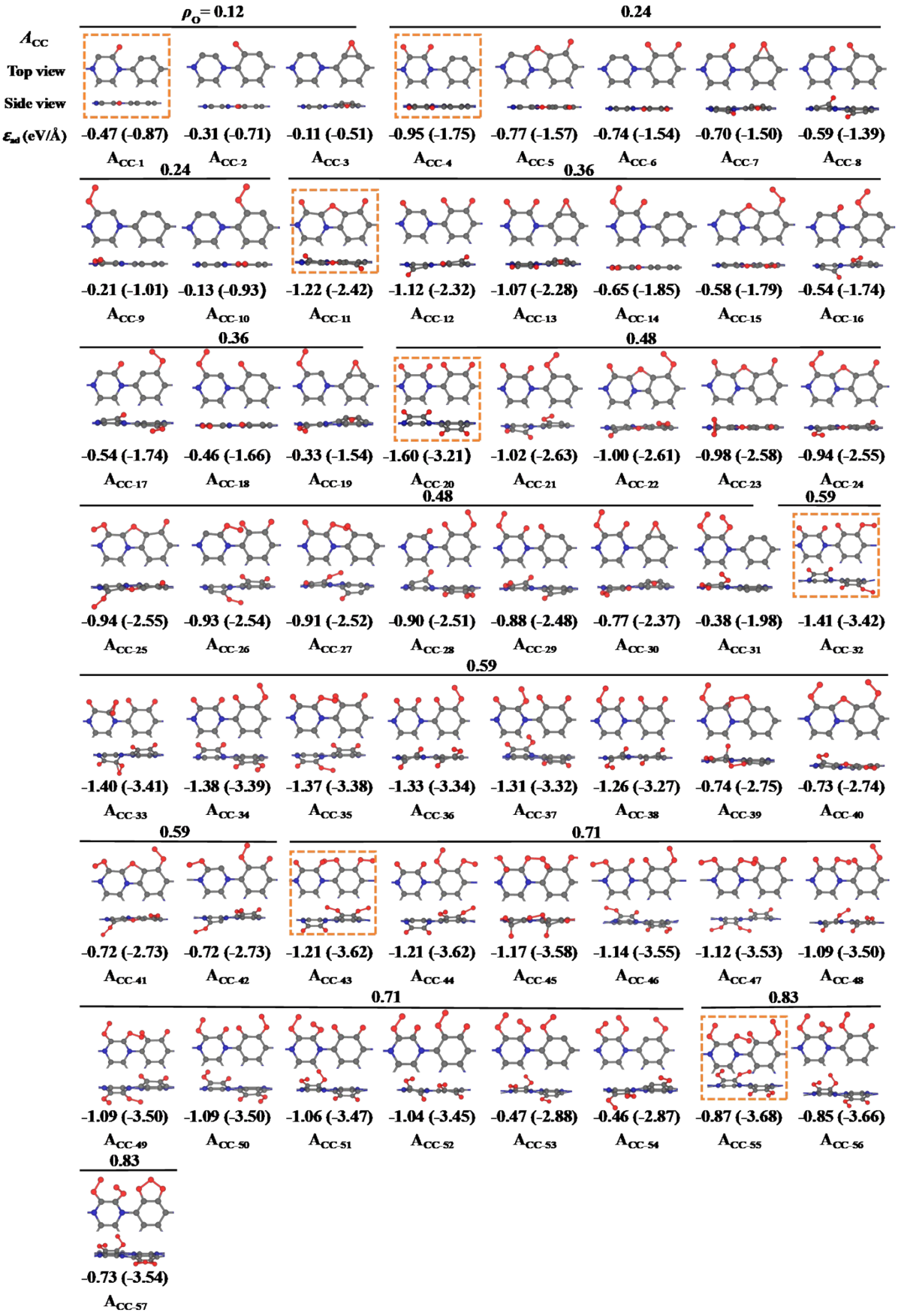
ρ_O = 0.12
0.24
A_{CC}
Top view
Side view
ε_{ad} (eV/Å)
-0.47 (-0.87)
-0.31 (-0.71)
-0.11 (-0.51)
-0.95 (-1.75)
-0.77 (-1.57)
-0.74 (-1.54)
-0.70 (-1.50)
-0.59 (-1.39)
A_{CC-1}
A_{CC-2}
A_{CC-3}
A_{CC-4}
A_{CC-5}
A_{CC-6}
A_{CC-7}
A_{CC-8}
0.24
0.36
-0.21 (-1.01)
-0.13 (-0.93)
-1.22 (-2.42)
-1.12 (-2.32)
-1.07 (-2.28)
-0.65 (-1.85)
-0.58 (-1.79)
-0.54 (-1.74)
A_{CC-9}
A_{CC-10}
A_{CC-11}
A_{CC-12}
A_{CC-13}
A_{CC-14}
A_{CC-15}
A_{CC-16}
0.36
0.48
-0.54 (-1.74)
-0.46 (-1.66)
-0.33 (-1.54)
-1.60 (-3.21)
-1.02 (-2.63)
-1.00 (-2.61)
-0.98 (-2.58)
-0.94 (-2.55)
A_{CC-17}
A_{CC-18}
A_{CC-19}
A_{CC-20}
A_{CC-21}
A_{CC-22}
A_{CC-23}
A_{CC-24}
0.48
0.59
-0.94 (-2.55)
-0.93 (-2.54)
-0.91 (-2.52)
-0.90 (-2.51)
-0.88 (-2.48)
-0.77 (-2.37)
-0.38 (-1.98)
-1.41 (-3.42)
A_{CC-25}
A_{CC-26}
A_{CC-27}
A_{CC-28}
A_{CC-29}
A_{CC-30}
A_{CC-31}
A_{CC-32}
0.59
-1.40 (-3.41)
-1.38 (-3.39)
-1.37 (-3.38)
-1.33 (-3.34)
-1.31 (-3.32)
-1.26 (-3.27)
-0.74 (-2.75)
-0.73 (-2.74)
A_{CC-33}
A_{CC-34}
A_{CC-35}
A_{CC-36}
A_{CC-37}
A_{CC-38}
A_{CC-39}
A_{CC-40}
0.59
0.71
-0.72 (-2.73)
-0.72 (-2.73)
-1.21 (-3.62)
-1.21 (-3.62)
-1.17 (-3.58)
-1.14 (-3.55)
-1.12 (-3.53)
-1.09 (-3.50)
A_{CC-41}
A_{CC-42}
A_{CC-43}
A_{CC-44}
A_{CC-45}
A_{CC-46}
A_{CC-47}
A_{CC-48}
0.71
0.83
-1.09 (-3.50)
-1.09 (-3.50)
-1.06 (-3.47)
-1.04 (-3.45)
-0.47 (-2.88)
-0.46 (-2.87)
-0.87 (-3.68)
-0.85 (-3.66)
A_{CC-49}
A_{CC-50}
A_{CC-51}
A_{CC-52}
A_{CC-53}
A_{CC-54}
A_{CC-55}
A_{CC-56}
0.83
-0.73 (-3.54)
A_{CC-57}

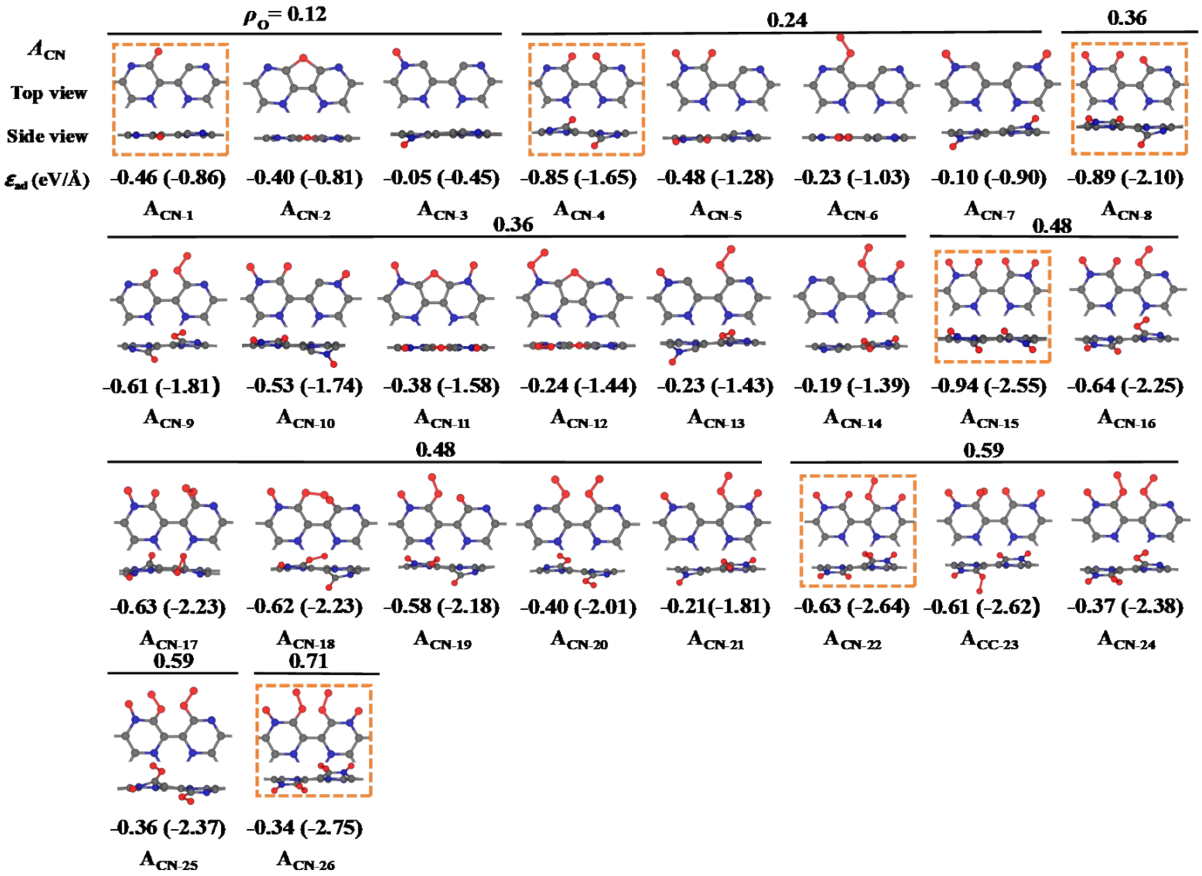
A_{CN}
Top view
Side view
ε_{ad} (eV/Å)
ρ_O= 0.12
0.24
0.36
-0.46 (-0.86)
A_{CN-1}
-0.40 (-0.81)
A_{CN-2}
-0.05 (-0.45)
A_{CN-3}
-0.85 (-1.65)
A_{CN-4}
-0.48 (-1.28)
A_{CN-5}
-0.23 (-1.03)
A_{CN-6}
-0.10 (-0.90)
A_{CN-7}
-0.89 (-2.10)
A_{CN-8}
0.36
0.48
-0.61 (-1.81)
A_{CN-9}
-0.53 (-1.74)
A_{CN-10}
-0.38 (-1.58)
A_{CN-11}
-0.24 (-1.44)
A_{CN-12}
-0.23 (-1.43)
A_{CN-13}
-0.19 (-1.39)
A_{CN-14}
-0.94 (-2.55)
A_{CN-15}
-0.64 (-2.25)
A_{CN-16}
0.48
0.59
-0.63 (-2.23)
A_{CN-17}
-0.62 (-2.23)
A_{CN-18}
-0.58 (-2.18)
A_{CN-19}
-0.40 (-2.01)
A_{CN-20}
-0.21(-1.81)
A_{CN-21}
-0.63 (-2.64)
A_{CN-22}
-0.61 (-2.62)
A_{CC-23}
-0.37 (-2.38)
A_{CN-24}
0.59
0.71
-0.36 (-2.37)
A_{CN-25}
-0.34 (-2.75)
A_{CN-26}

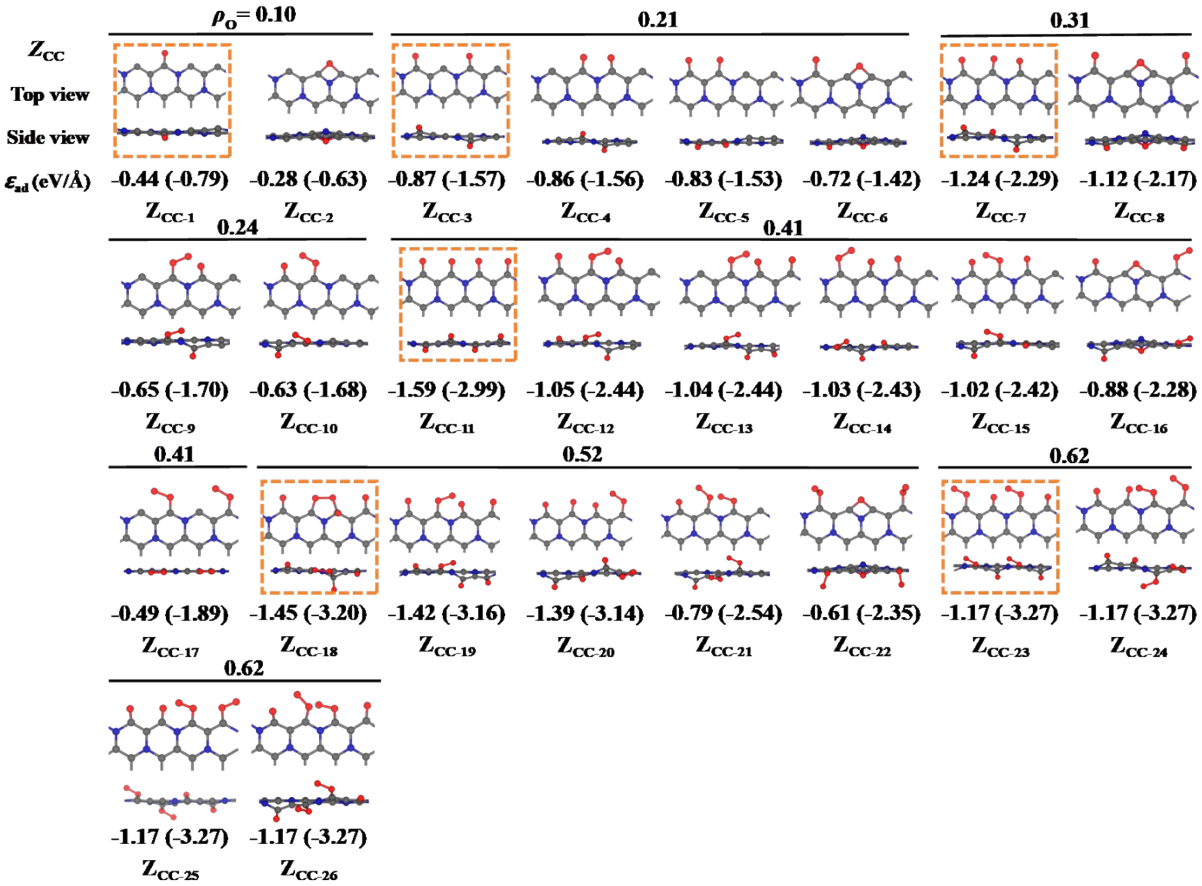
Z_{CC}
Top view
Side view
ε_{ad} (eV/Å)
ρ_O= 0.10
0.21
0.31
-0.44 (-0.79)
Z_{CC-1}
-0.28 (-0.63)
Z_{CC-2}
-0.87 (-1.57)
Z_{CC-3}
-0.86 (-1.56)
Z_{CC-4}
-0.83 (-1.53)
Z_{CC-5}
-0.72 (-1.42)
Z_{CC-6}
-1.24 (-2.29)
Z_{CC-7}
-1.12 (-2.17)
Z_{CC-8}
0.24
0.41
-0.65 (-1.70)
Z_{CC-9}
-0.63 (-1.68)
Z_{CC-10}
-1.59 (-2.99)
Z_{CC-11}
-1.05 (-2.44)
Z_{CC-12}
-1.04 (-2.44)
Z_{CC-13}
-1.03 (-2.43)
Z_{CC-14}
-1.02 (-2.42)
Z_{CC-15}
-0.88 (-2.28)
Z_{CC-16}
0.41
0.52
0.62
-0.49 (-1.89)
Z_{CC-17}
-1.45 (-3.20)
Z_{CC-18}
-1.42 (-3.16)
Z_{CC-19}
-1.39 (-3.14)
Z_{CC-20}
-0.79 (-2.54)
Z_{CC-21}
-0.61 (-2.35)
Z_{CC-22}
-1.17 (-3.27)
Z_{CC-23}
-1.17 (-3.27)
Z_{CC-24}
0.62
-1.17 (-3.27)
Z_{CC-25}
-1.17 (-3.27)
Z_{CC-26}

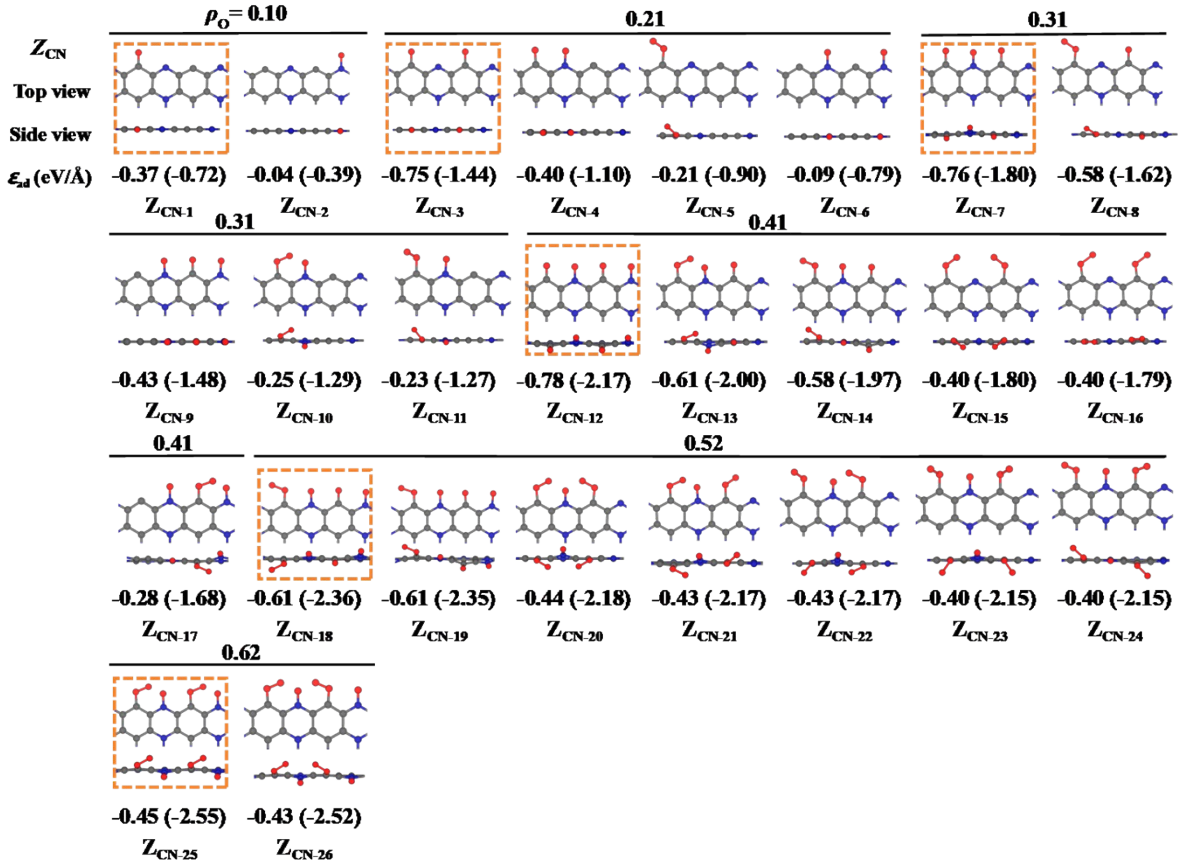

Figure S2. All the 135 optimized configurations of four distinct oxidized edges, denoted by A_{CC}, A_{CN}, Z_{CC} and Z_{CN}, at various oxygen densities ρ_O. The numbers above the black line and below the configurations represent the ρ_O and ε_{ad}, respectively. The configurations below the same horizontal black line have the same value of ρ_O and they are sorted by increasing the ε_{ad}. The orange dash frame highlights the configuration with the lowest ε_{ad}. The value of ε_{ad} inside or outside the bracket is calculated with reference to the atomic O or O_2 state. Only edge atoms are shown here for clarity.

PS. 3. Averaged height deviations of edge O atoms for four types of C_3NNR edges

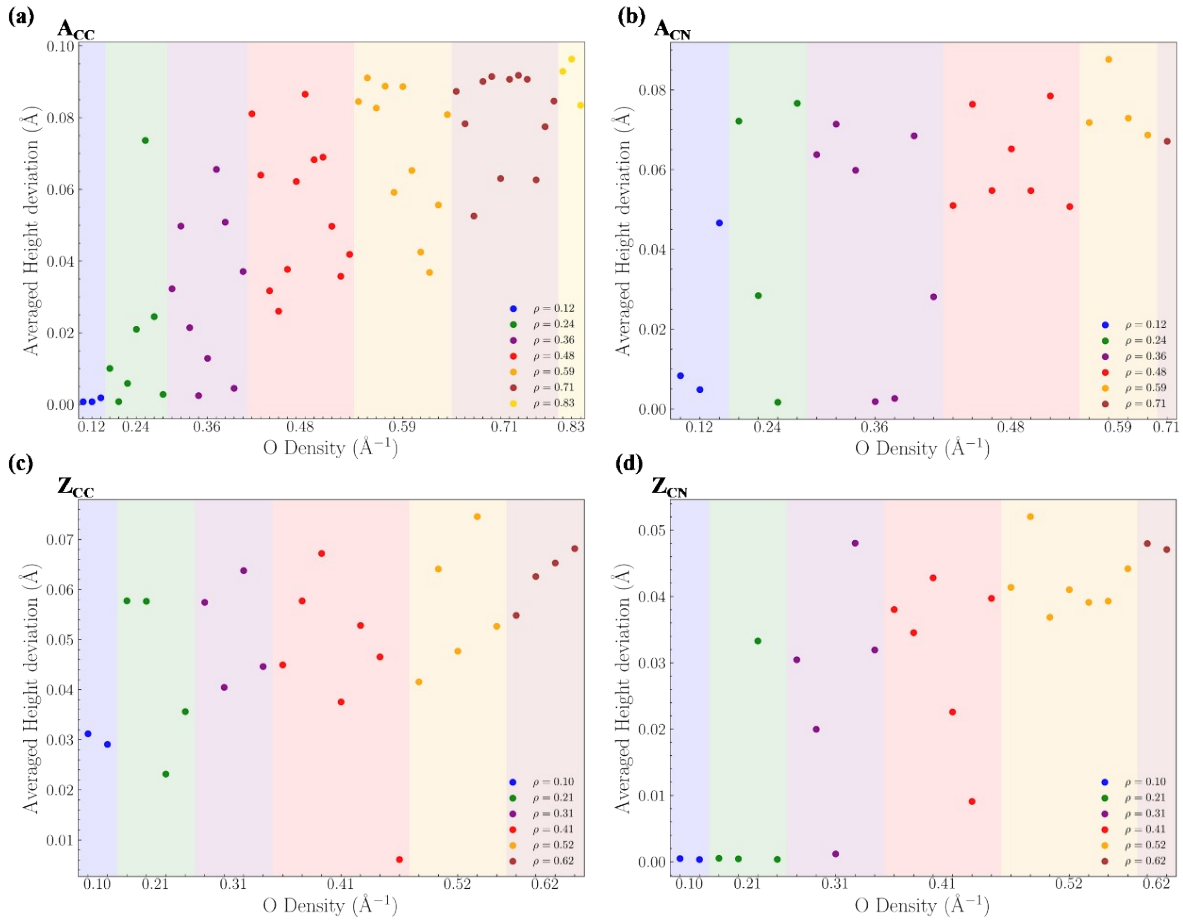

Figure S3. Averaged height deviations of edge O atoms from the C_3N plane, $\bar{d}$, with respect to oxygen density ρ_O, for four types of C_3NNR edges denoted by (a) A_{CC}, (b) A_{CN}, (c) Z_{CC} and (d) Z_{CN}. The $\bar{d}$ is defined by the average value of all the vertical distances of the edge O atoms from the C_3N plane. For each edge type, all the oxidation configurations are considered for analysis and the scatter dots belonging to the same O density is covered by transparent shaded area.

PS. 4. Bond lengths of edge atoms during edge oxidation in AIMD for four types of C_3NNR edges

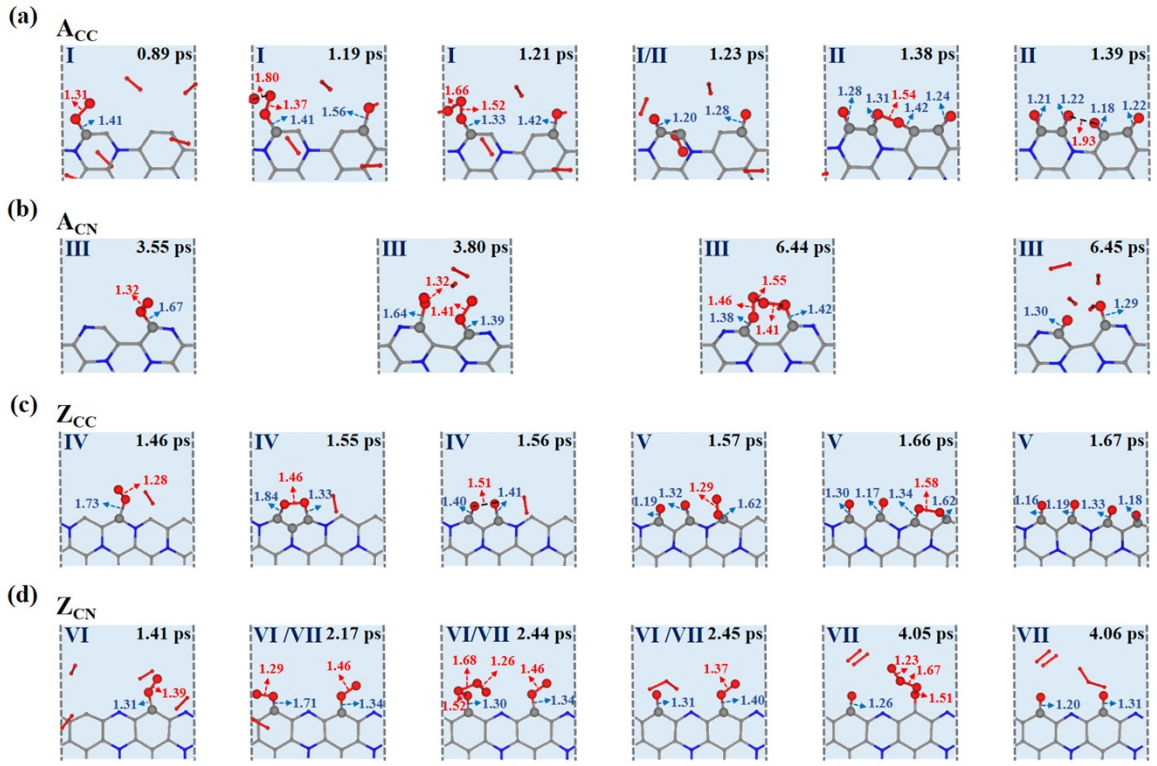

Figure S4. Bond lengths of edge atoms during edge oxidation in AIMD simulations for four types of C_3NNR edges, denoted by (a) A_{CC}, (b) A_{CN}, (c) Z_{CC} and (d) Z_{CN}. The carbon-oxygen, oxygen-oxygen bonds are shown by blue and red numbers in the unit of Å. In each snapshot, upper right number denotes the time. Snapshots with the same upper left characters belong to the same oxidation stage. The oxidized sites and the adsorbed atomic O or O_2 are shown in balls to highlight the oxidation process. Only the edge atoms in the main system are shown within two gray dashed lines for clarity.

PS. 5. Electronic band structure and DOS of the most stable oxidized configurations for four types of C_3NNR edges

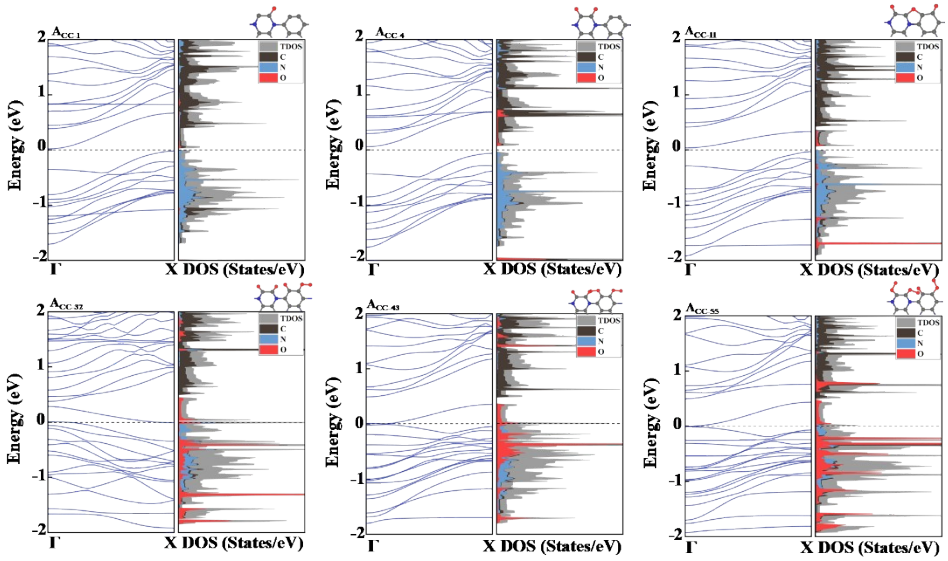

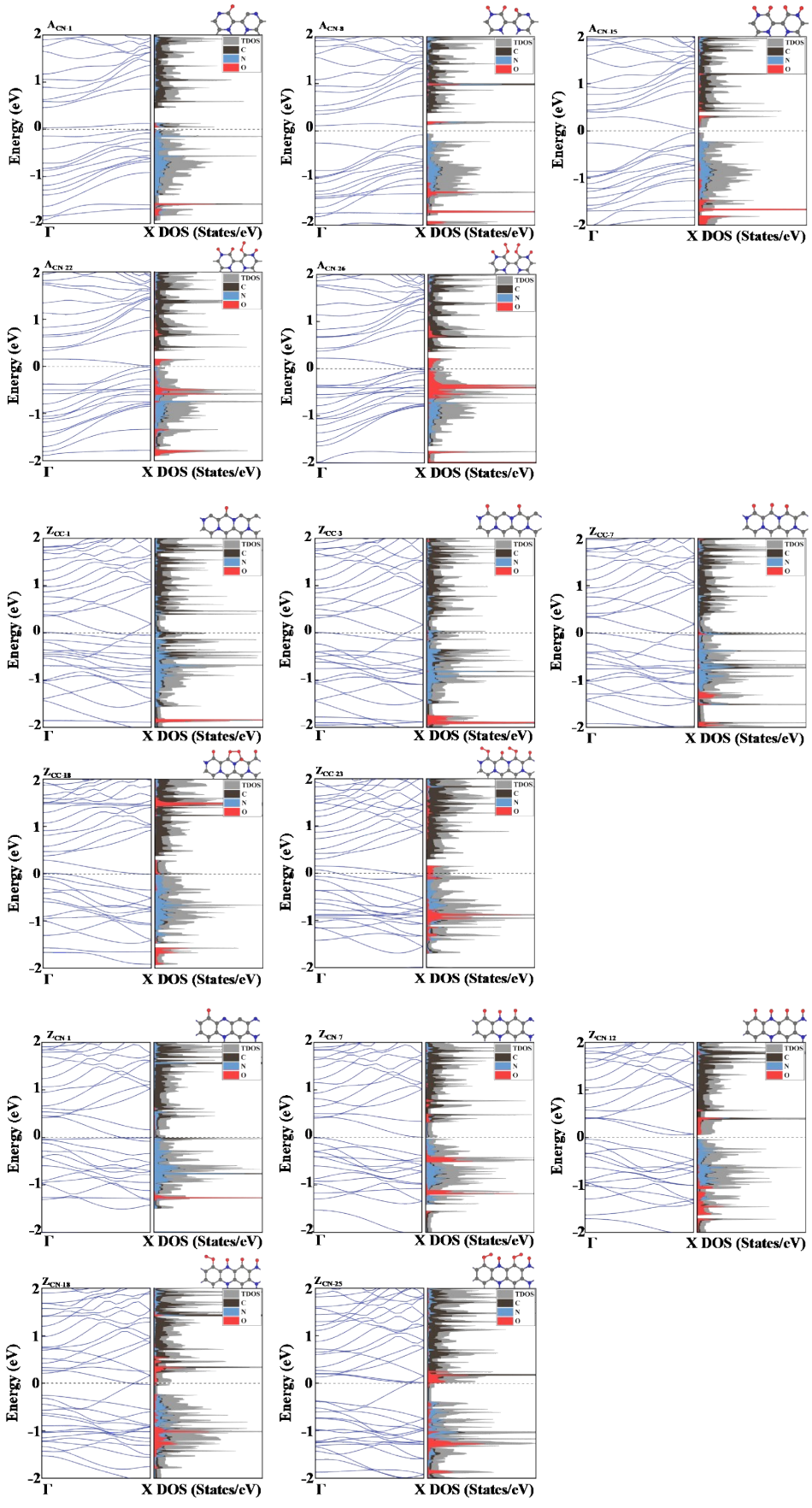
A_CN-1
A_CN-8
A_CN-15
A_CN-22
A_CN-26
Z_CC-1
Z_CC-3
Z_CC-7
Z_CC-18
Z_CC-23
Z_CN-1
Z_CN-7
Z_CN-12
Z_CN-18
Z_CN-25
TDOS
C
N
O
Energy (eV)
Γ
X
DOS (States/eV)

Figure S5. Electronic band structure and DOS of the most stable oxidation configurations at different oxygen densities for four types of C_3NNR edges. The results for A_{CC-20}, A_{CN-4}, Z_{CC-11} and Z_{CN-3} have been shown as Figure 7 in the manuscript.